J Solid State Electrochem (2005) 9: 483–497
DOI 10.1007/s10008-004-0584-z

ORIGINAL PAPER

Ksenija Babić-Samardžija · Norman Hackerman

Triazole, benzotriazole and substituted benzotriazoles as corrosion inhibitors of iron in aerated acidic media

Received: 14 June 2004 / Revised: 13 July 2004 / Accepted: 5 August 2004 / Published online: 21 January 2005

Abstract The effect of a 1*H*-1,2,3-triazole, 1,2,3-benzotriazole and a number of substituted benzotriazoles, namely 1-hydroxybenzotriazole, 1*H*-benzotriazole-1-methanol and *N*-(1*H*-benzotriazol-1-ylmethyl)-formamide, have been investigated with respect to the corrosion of iron in 1 mol/l HCl and 1 mol/l $HClO_4$. The Tafel extrapolation method, linear polarization resistance and electrochemical impedance spectroscopy illustrate the inhibiting effect of all of these compounds in both acids. They are better inhibitors in 1 mol/l HCl than in 1 mol/l $HClO_4$. The changes of charge transfer resistance are also indicative for adsorption and inhibition of all of these compounds. This effect increases with time up to 16 h. An equivalent circuit is suggested as a model for the impedance. The adsorption of triazole-type of compounds in both acids follows a Langmuir isotherm. Molecular modeling was used to gain some insight, about structural and electronic effects in relation to the inhibiting efficiencies.

Keywords Benzotriazoles · Acid solutions · Iron · Inhibition

Introduction

Corrosion of metals in acidic solutions is usually electrochemical process in nature, influenced by various environmental factors [1]. Since acidic solutions are widely used in industry, corrosion inhibitors are needed to reduce metallic corrosion. They are mostly organic compounds containing one or more heteroatom, multiple bonds or aromatic ring(s) [2, 3, 4, 5, 6, 7, 8]. The inhibitive action of such compounds is related to the presence of atom(s) with unshared electron pairs, available for adsorption to the metal thereby slowing the corrosion process [6, 7, 8, 9, 10].

Nitrogen-containing compounds of the triazole-type were showed as effective inhibitors for many metals and alloys [2, 4, 5, 6, 7] due to the presence of three nitrogen atoms in an aromatic ring. It is known that benzotriazole is an effective inhibitor for Cu [11, 12, 13, 14] and Fe [15]. Surface-enhanced Raman spectroscopy shows that benzotriazole interacts with iron through its triazole ring [15]. The surface complex $[Fe_n(Cl)_p(BZT)]_m$ formed by the participation of the chloride ion is present in that solution. The adsorption is believed to occur by coordination through the lone electron pair on one of the nitrogens with an iron atom.

We thought it would be interesting to investigate benzotriazole compounds with some oxygen-containing substituents. Its tendency to form coordinate bond might be enhanced by increasing the effective electronic density of the functional group.

Electrochemical methods used here were Tafel extrapolation and polarization resistance measurements. They are DC corrosion techniques, the first by extrapolation of the applied current from the anodic and cathodic region to the open-circuit potential, and the second by anodic and cathodic polarization within vicinity ± 25 mV of the corrosion potential, i.e., applied current density is approximately linear with potential. Also, an AC electrochemical impedance technique is used as a complex number in terms of a magnitude and a phase shift, available for identifying corrosion reaction mechanism [16]. Molecular orbital calculations based on the semi-empirical PM3 method [17] were performed for all compounds in order to get better insight into their structural and electronic properties, and correlate this with their inhibitor efficiency.

Materials and methods

Experiments were carried out on iron rod with a surface area 0.28 cm^2 (Puratronic 99.99%, Johnson

K. Babić-Samardžija (✉) · N. Hackerman
Chemistry Department MS60, Rice University,
6100 Main St., Houston, TX 77005, USA
E-mail: kbabic@rice.edu

Matthey Company) mounted in Teflon. The iron surface was prepared before each experiment using emery papers of different grit sizes down to 4/0 grit, polished with Al_2O_3 (0.5 μm particle size) and cleaned in an 18 MΩ water bath. The electrode was rinsed with acetone and bi-distilled water, and dried at room temperature.

A three-electrode component electrochemical cell was used. A saturated calomel electrode (SCE) served as a reference, platinum wire (Premion 99.997%) and 99.9% platinum gauze (52 mesh, Johnson Matthey Company) as counter and working iron electrode, respectively. The experiments were carried out in an open cell under static aerated conditions, at 25 °C, with a fine Lugin capillary placed close to the working electrode to minimize ohmic resistance.

Hydrochloric and perchloric acid (Fisher Scientific) solutions were prepared from concentrated acid and bi-distilled water. The organic compounds (TCI America) were used without any pretreatment. Fresh solutions were prepared before each experiment. Structures of all compounds investigated are shown in Fig. 1.

Measurements were performed with a Gamry Instrument Potentiostat/Galvanostat /ZRA. This includes a Gamry Framework system based on the ESA400 and the VFP600, and Gamry applications that include DC105 corrosion and EIS300 electrochemical impedance spectroscopy measurements, along with a computer for collecting the data. Echem Analyst 4.0 software was used for plotting, graphing and fitting data. Impedance time experiments were done with a Solartron 1250 frequency response analyzer using EIS software model 398 for data analysis.

The Tafel curves were obtained by changing the electrode potential automatically from −250 mV to +250 mV vs open circuit potential (E_{oc}) at a scan rate of 1 mV/s. Linear polarization resistance experiments were done at −25 mV to +25 mV vs E_{oc} at a scan rate of 1 mV/s. Electrochemical impedance spectroscopy (EIS) measurements were carried out under potentiostatic conditions in a frequency range of 100 kHz to 0.1 Hz with an amplitude of 1 mV peak-to-peak using AC signals at open circuit potential. All experiments were measured after 900 s immersion time. EIS time experiments were carried out after 7200 s immersion time in the same frequency range, with amplitude of 5 mV peak-to-peak using AC signals at E_{oc}.

Molecular modeling was carried out with Hyperchem version 7, a quantum mechanical program marketed by Hypercube Inc., implemented on an Intel Pentium 3, 600-MHz computer. The PM3 method [17] used is based on the semi-empirical Self-Consistent Field Molecular Orbital (SCF-MO) method [18, 19]. A full optimization of all geometrical variables without any symmetry constraint was performed at the Restricted Hartree-Fock level [20, 21].

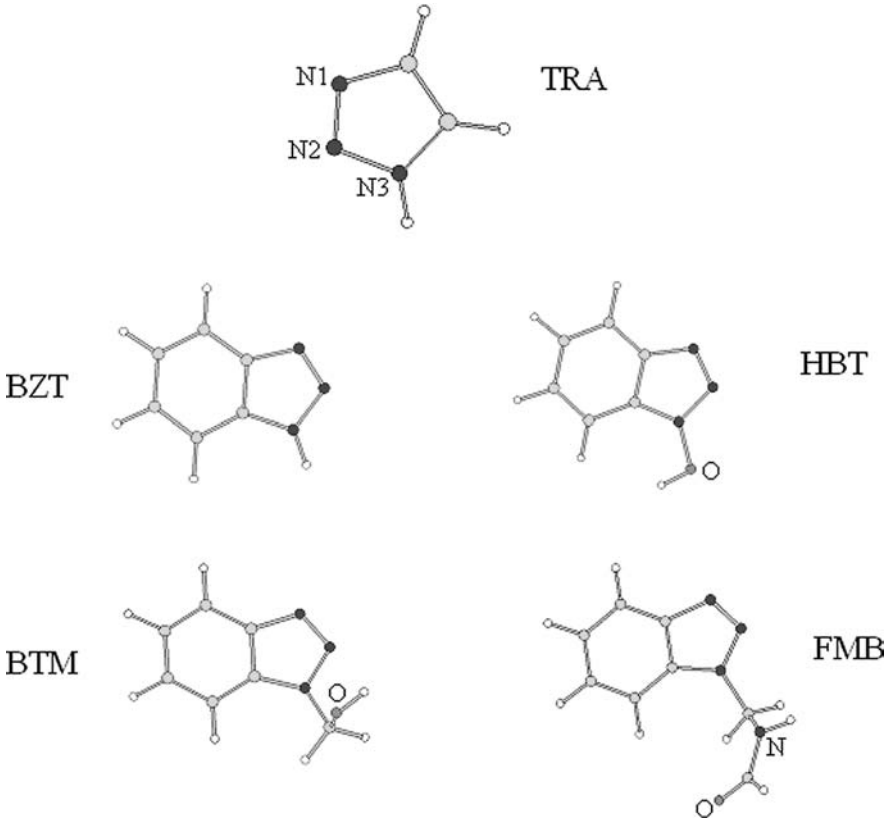

Fig. 1 Optimized structures (SCF-MO PM3 method) for triazole (TRA), benzotriazole (BZT), 1-hydroxybenzotriazole (HBT), 1*H*-benzotriazol-1-methanol (BTM) and *N*-(1*H*-benzotriazole-1-ylmethyl)-formamide (FMB)

Results and discussion

Tafel extrapolation

Tafel data for iron immersed in 1 mol/l HCl in the absence and presence of inhibitors are given in Table 1. The potential/current Tafel lines are shown in Fig. 2. The corrosion current (i_{corr}), corrosion potential (E_{corr}) as well as cathodic (β_c) and anodic (β_a) slopes were determined by extrapolation. Inhibitor efficiency (IE) was calculated using the equation

$$IE = \left(\frac{i^o_{corr} - i_{corr}}{i^o_{corr}}\right) \times 100 \quad (1)$$

where i^o_{corr} and i_{corr} correspond to current densities of uninhibited and inhibited solutions, respectively. i_{corr} was used to calculate a corrosion rate (CR) of iron:

$$CR = \frac{i_{corr} KEw}{dA} \quad (2)$$

where K is a constant that defines the units for the CR (3272 mm/A cm year) and A, d, and Ew are sample area, density and equivalent weight of iron, respectively.

In 1 mol/l HCl, both i_{corr} and CR decreased considerably with inhibitor. The corrosion inhibition of triazole, benzotriazole and derivatives are all in a relatively small efficiency range. At the highest inhibitor concentration, 10^{-2} mol/l, the inhibiting effect is often in excess 88% (Table 1).

The compounds affect both electrochemical processes i.e. the anodic dissolution of iron and the hydrogen reduction processes. In their presence corrosion of iron is under 'mixed' control, with TRA and BZT (Fig. 2a) and HBT, BTM and FMB (Fig. 2b).

Similar behavior is observed for iron in 1 mol/l $HClO_4$ acid. Typical Tafel curves as well as kinetic parameters are shown in Fig. 3 and Table 2. Again, the presence of triazole-type compounds decrease rate of corrosion, decrease current density and increase inhibitor efficiency (Table 2) but less so than in HCl (Table 1). The inhibiting effect increases with concentration as for HCl. The largest effect in 1 mol/l $HClO_4$ shows BZT (Fig. 3) at 10^{-2} mol/l, at 80% efficiency.

Comparing inhibitor behaviors in both acids, it is evident that in 1 mol/l $HClO_4$ the corrosion potential is shifted anodically and in 1 mol/l HCl cathodically by these inhibitors, but there is no definite trend found in potentials (Tables 1 and 2). In both acids, increasing the inhibitor concentration decreases current densities. The slopes β_a and β_c change both electrode reaction, and their shift depends on inhibitor concentration. The addition of triazole, benzotriazole and derivatives inhibit anodic and cathodic reactions on the iron indicating their inhibitor performance of mixed type.

The effect of inhibitor concentration and Tafel slope CR is shown in Fig. 4. The greater increase in inhibiting behavior is observed with BTM and FMB (Fig. 4a). The highest efficiency is found for BTM, where both electrochemical reactions are decreased the most (Fig. 2b) and lowest corrosion rate is obtained (Table 1). Compared to the other substituted benzotriazole derivatives this effect is probably due to increased electronic transfer from its functional group. However, variation in inhibitor efficiency also depends on the nature of the R-groups on the aromatic ring [3] (Fig. 1). Normally, oxygen-containing substituents are expected to affect electron charge density on the active center of the molecule and thus improve inhibition [22].

Table 1 Electrochemical kinetic parameters of iron corrosion in 1 mol/l HCl without and with different concentrations of inhibitors

Compound	Conc. M	i_{corr} μA/cm^2	$-E_{corr}$ mV	β_a mV/dec	β_c mV/dec	IE %	CR mpy
Fe/1 mol/l HCl	-	169.5	503.3	132.7	206.6	-	277.0
TRA	10^{-4}	93.32	505.7	132.2	169.9	44.94	152.5
	10^{-3}	80.67	526.7	120.1	248.3	52.40	131.8
	5×10^{-3}	41.52	533.5	105.3	172.6	75.50	67.8
	10^{-2}	29.74	535.0	100.9	175.7	82.45	48.6
BZT	10^{-4}	71.18	518.8	115.6	284.3	58.01	116.3
	10^{-3}	65.66	519.3	110.8	271.0	61.26	107.3
	5×10^{-3}	34.65	534.0	113.3	197.8	79.55	56.6
	10^{-2}	26.54	533.7	106.0	166.1	84.34	43.4
HBT	10^{-4}	73.60	509.8	110.8	274.1	56.57	120.3
	10^{-3}	67.04	510.5	103.2	263.9	60.45	109.5
	5×10^{-3}	39.39	506.2	94.6	248.1	76.76	64.4
	10^{-2}	28.69	524.4	96.9	199.6	83.07	46.9
BTM	10^{-4}	55.68	520.8	120.9	204.2	67.15	90.9
	10^{-3}	37.91	515.1	100.5	211.4	77.63	61.9
	5×10^{-3}	32.05	513.0	99.9	203.8	81.09	52.4
	10^{-2}	20.59	508.5	87.8	164.5	87.85	33.6
FMB	10^{-4}	69.80	528.3	116.0	251.3	58.82	114.1
	10^{-3}	45.93	530.3	117.2	220.2	72.90	75.0
	5×10^{-3}	33.06	507.5	94.1	194.0	80.49	54.0
	10^{-2}	22.24	510.1	90.2	165.1	86.88	36.3

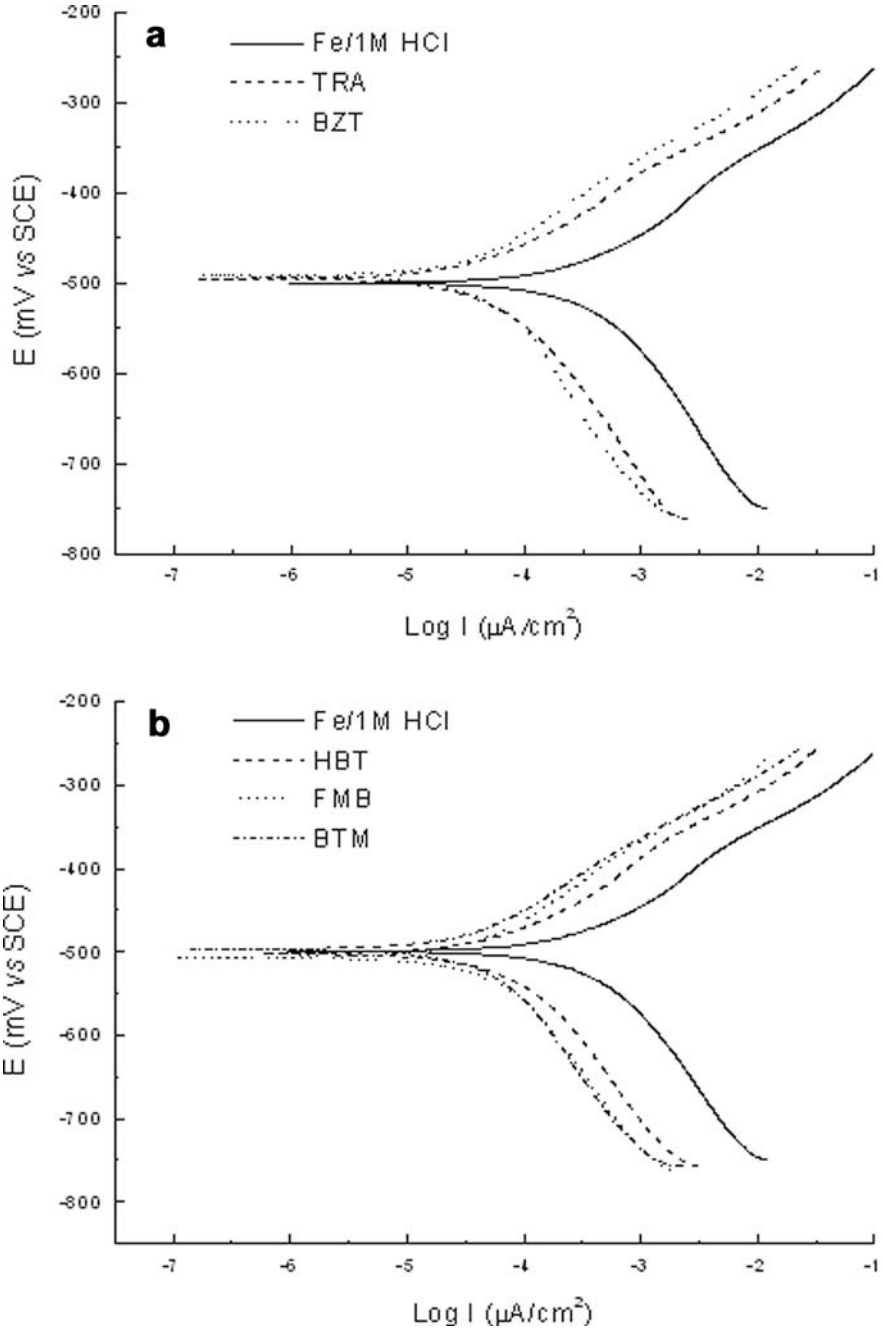

Fig. 2a,b Anodic and cathodic Tafel lines for iron in uninhibited 1 mol/l HCl and with addition of inhibitors: **a** TRA and BZT at concentration 10^{-3} mol/l; **b** HBT, FMB and BTM at concentration 5×10^{-3} mol/l

Linear polarization resistance

Electrochemical corrosion kinetic parameters obtained from polarization resistance (R_p) for both acids, 1 mol/l HCl and 1 mol/l $HClO_4$ in the presence and absence of triazole, benzotriazole and derivatives are given in Tables 3 and 4, respectively.

The scan through a potential range of ± 25 mV at open circuit potential gives a linear current response. This slope and intersection gives R_p and E_{corr} values, respectively. i_{corr} was calculated (Tables 3 and 4) by applying Eq. (3) for charge transfer controlled reaction kinetics for the case of small corrosion potential perturbation [23]:

$$i_{corr} = \left(\frac{\beta_a \beta_c}{2.303(\beta_a + \beta_c)}\right) \times \left(\frac{1}{R_p}\right) \tag{3}$$

where β_a and β_c are anodic and cathodic slopes, respectively.

Inhibition efficiency is calculated from Eq. (4):

$$IE = \left(1 - \frac{R_p^o}{R_p}\right) \times 100 \tag{4}$$

where R_p^o and R_p represent polarization resistance for uninhibited and inhibited solution, respectively.

The values of R_p in both acids show that polarization resistance increased with increasing concentration of

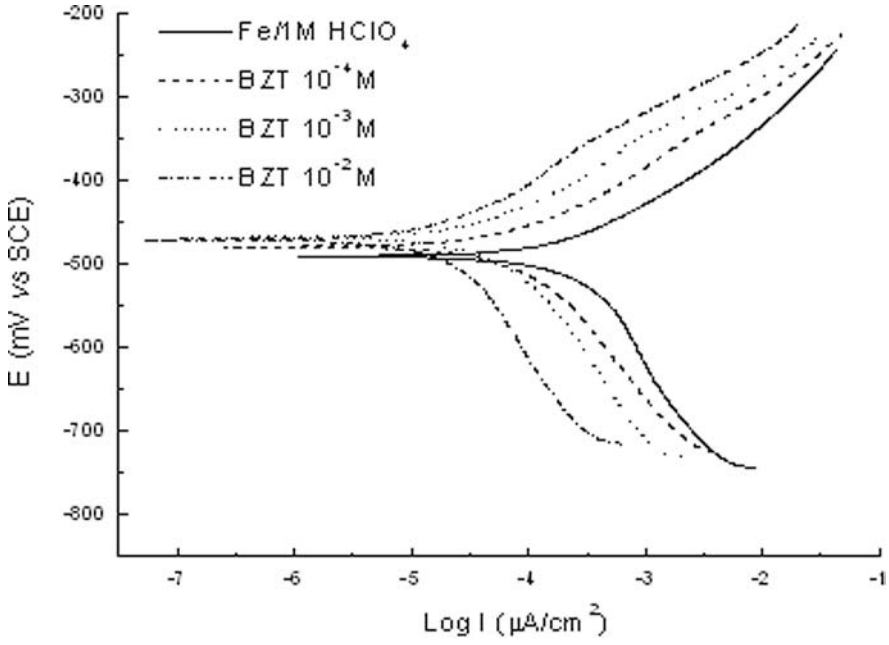

Fig. 3 Anodic and cathodic Tafel lines for iron in uninhibited 1 mol/l $HClO_4$ and with addition of BZT at concentration range of 10^{-4} to10^{-2} mol/l

Table 2 Electrochemical kinetic parameters of iron corrosion in 1 mol/l $HClO_4$ without and with different concentrations of inhibitors

Compound	Conc. M	i_{corr} μA/cm^2	$-E_{corr}$ mV	β_a mV/dec	β_c mV/dec	IE %	CR mpy
Fe/1 mol/l $HClO_4$	-	91.88	506.9	102.1	147.0	-	150.1
TRA	10^{-4}	54.11	475.6	85.13	170.5	41.11	88.4
	10^{-3}	48.94	479.3	83.16	170.0	46.73	79.9
	5×10^{-3}	38.06	468.0	77.94	171.4	58.57	62.2
	10^{-2}	28.50	463.3	74.58	111.1	68.98	46.5
BZT	10^{-4}	36.79	472.9	76.81	177.8	59.96	60.1
	10^{-3}	31.56	483.4	78.24	166.1	65.65	51.6
	5×10^{-3}	28.97	469.2	74.38	178.5	68.47	47.3
	10^{-2}	18.77	463.9	66.68	142.2	79.57	30.6
HBT	10^{-4}	79.33	455.4	83.30	313.8	13.66	129.6
	10^{-3}	64.54	440.3	77.39	368.1	29.75	105.5
	5×10^{-3}	41.86	448.5	74.37	300.2	54.44	68.4
	10^{-2}	32.13	439.6	73.10	222.4	65.03	52.5
BTM	10^{-4}	46.66	456.8	73.08	269.1	49.21	76.2
	10^{-3}	44.76	444.7	72.90	267.8	51.28	73.1
	5×10^{-3}	37.23	443.9	71.50	264.3	59.48	60.8
	10^{-2}	26.43	443.8	69.21	214.5	71.23	43.3
FMB	10^{-4}	42.30	468.7	79.29	217.0	53.96	69.1
	10^{-3}	36.08	468.5	76.50	198.3	60.73	58.9
	5×10^{-3}	31.60	482.1	77.59	213.4	65.61	51.6
	10^{-2}	22.78	474.9	72.53	172.2	75.20	37.2

inhibitor. Electrochemical kinetic parameters are in satisfactory correlation for both DC methods (Tables 1, 2, 3, 4 and Fig. 5), with the same order of inhibitor efficiency obtained by both.

Electrochemical impedance spectroscopy

All impedance measurements were performed under potentiostatic conditions. Nyquist plots of uninhibited and inhibited solutions in 1 mol/l HCl are shown in Fig. 6. Charge transfer resistance (R_{ct}) was calculated from the difference in impedance at the lower and higher frequencies. The impedance diagrams are not perfect semicircles, which can be attributed to frequency dispersion [13]. It is evident from Nyquist plots that they are significantly changed on addition of inhibitors (Fig. 6).

Figure 7 shows that the impedance of the inhibited system increased with inhibitor concentration. For all compounds investigated in 1 mol/l HCl, Fig. 7a shows a big gap between the first and second concentration used and an almost linear increase behind. The inhibiting effect is lesser in 1 mol/l $HClO_4$ compared with that in 1 mol/l HCl. Also, in 1 mol/l $HClO_4$ the inhibiting effect of HBT remains unchanged above 10^{-3} mol/l, while BZT increase in this range.

R_{ct} values for 2–16 h of immersion time at the highest inhibitor concentration are presented in Fig. 8. These

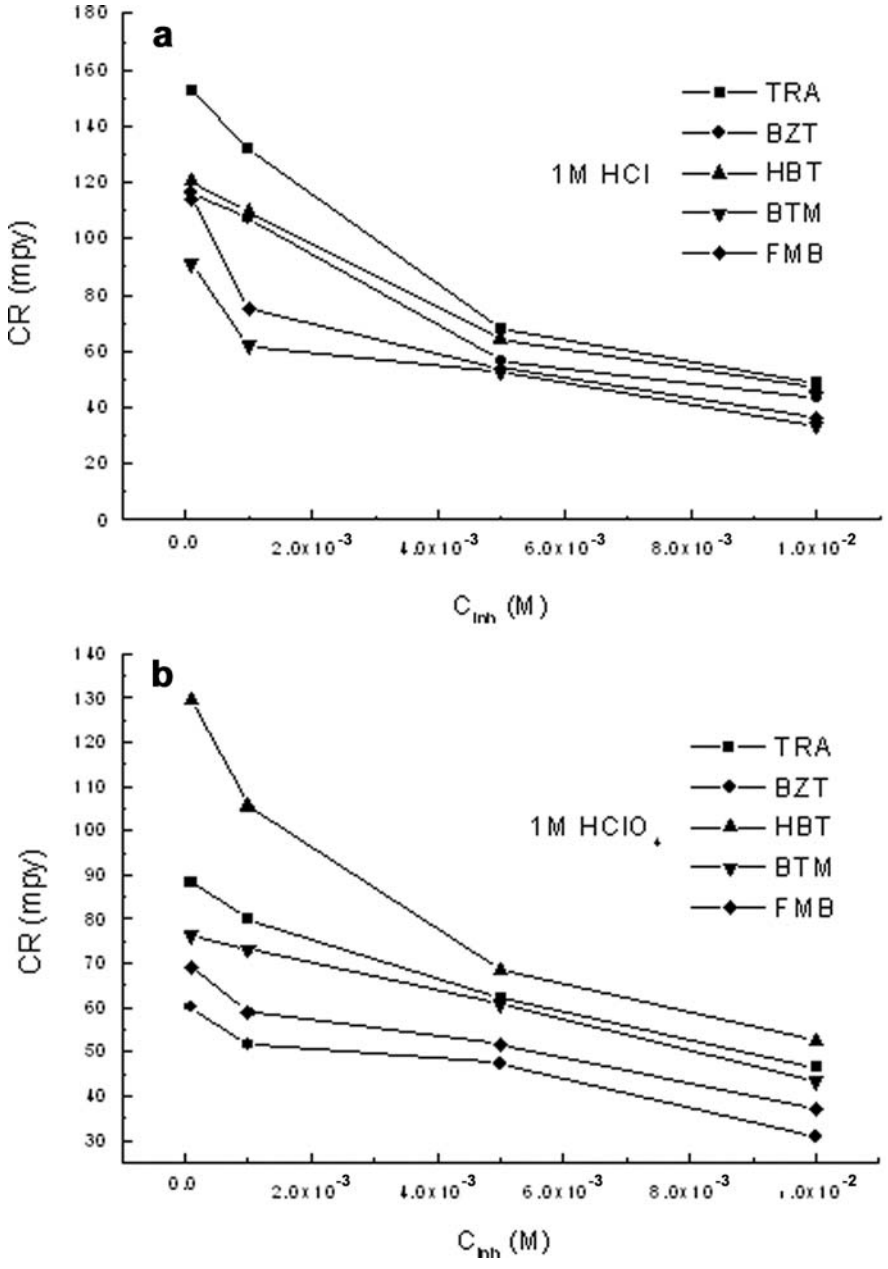

Fig. 4a,b Correlation between Tafel slope corrosion rate and inhibitor concentration in: **a** 1 mol/l HCl; **b** 1 mol/l $HClO_4$

results show increased charge transfer resistance over the 16 h and enhanced inhibiting effect. It is indicative that after 10–12 h of immersion time the inhibiting effect is almost constant.

An electrical equivalent circuit is generally used to model the electrochemical behavior and to calculate some parameters of interest. The equivalent circuit in Fig. 9 fits the impedance data well. This model represents one possible assignment of circuit elements to physical phenomena on a metal surface.

The impedance spectra described by semicircles are indicative for single charge transfer reaction occurring with R_{ct} parallel with the interfacial capacitance, replaced with CPE [24]. R_s, R_{ct} and CPE refer to solution resistance, charge transfer resistance and constant phase element, respectively. For the description of a frequency independent phase shift between an applied AC potential and its current response, the impedance of a CPE has the form

$$Z = \frac{\frac{1}{Z_o}}{(j\omega)^{\alpha}} \tag{5}$$

where Z_o is the CPE constant, ω is the angular frequency and j is the imaginary number. When this equation describes a capacitor, the constant $Z_o = C$ (the capacitance) and the exponent $\alpha = 1$. For a constant phase element, the exponent $\alpha < 1$.

Using the concept of CPE we got excellent fit for all experimental data. Representative examples of Nyquist

Table 3 Polarization resistance data of iron in 1 mol/l HCl in the absence and presence of different concentrations of inhibitors

Compound	Conc. M	R_p Ω/cm^2	i_{corr} $\mu A/cm^2$	$-E_{corr}$ mV	IE %
Fe/1 mol/l HCl	-	160.6	162.2	507.2	-
TRA	10^{-4}	275.7	94.5	506.8	41.7
	10^{-3}	321.6	81.0	497.2	50.1
	5×10^{-3}	624.1	41.7	534.3	74.2
	10^{-2}	829.7	31.4	537.0	80.6
BZT	10^{-4}	371.9	70.0	495.8	56.8
	10^{-3}	389.1	66.9	512.1	58.7
	5×10^{-3}	683.2	38.1	541.1	76.5
	10^{-2}	950.0	27.4	515.9	83.1
HBT	10^{-4}	358.0	72.7	495.4	55.1
	10^{-3}	391.8	66.5	510.7	59.0
	5×10^{-3}	605.4	43.0	516.8	73.5
	10^{-2}	902.3	28.8	548.2	82.2
BTM	10^{-4}	407.8	63.9	528.1	60.6
	10^{-3}	684.2	38.1	524.0	76.5
	5×10^{-3}	797.0	32.7	522.9	79.8
	10^{-2}	1263	20.6	542.0	87.3
FMB	10^{-4}	396.5	65.7	500.5	59.5
	10^{-3}	593.6	43.9	527.6	72.9
	5×10^{-3}	789.8	32.9	539.0	79.6
	10^{-2}	1110	23.4	518.0	85.5

Table 4 Polarization resistance data of iron in 1 mol/l $HClO_4$ in the absence and presence of different concentrations of inhibitors

Compound	Conc. M	R_p Ω/cm^2	i_{corr} $\mu A/cm^2$	$-E_{corr}$ mV	IE %
Fe/1 mol/l $HClO_4$	-	235.7	110.5	516.8	-
TRA	10^{-4}	474.9	54.8	465.3	50.4
	10^{-3}	538.7	48.4	475.2	56.2
	5×10^{-3}	629.5	41.4	459.3	62.5
	10^{-2}	949.8	27.4	449.3	75.2
BZT	10^{-4}	722.9	36.0	489.8	67.4
	10^{-3}	817.6	31.8	500.2	71.2
	5×10^{-3}	935.5	27.8	480.7	74.8
	10^{-2}	1030	25.3	484.6	82.4
HBT	10^{-4}	355.6	73.3	461.9	33.7
	10^{-3}	410.7	63.4	451.6	42.6
	5×10^{-3}	611.8	42.6	488.1	61.5
	10^{-2}	727.8	35.8	448.7	67.6
BTM	10^{-4}	540.4	48.2	480.7	56.4
	10^{-3}	558.0	46.7	465.8	57.7
	5×10^{-3}	743.4	35.1	455.6	68.3
	10^{-2}	985.6	26.4	495.1	76.1
FMB	10^{-4}	629.6	41.4	482.6	62.5
	10^{-3}	665.1	39.2	465.6	64.5
	5×10^{-3}	827.0	31.5	481.2	71.5
	10^{-2}	1018	25.6	480.2	76.8

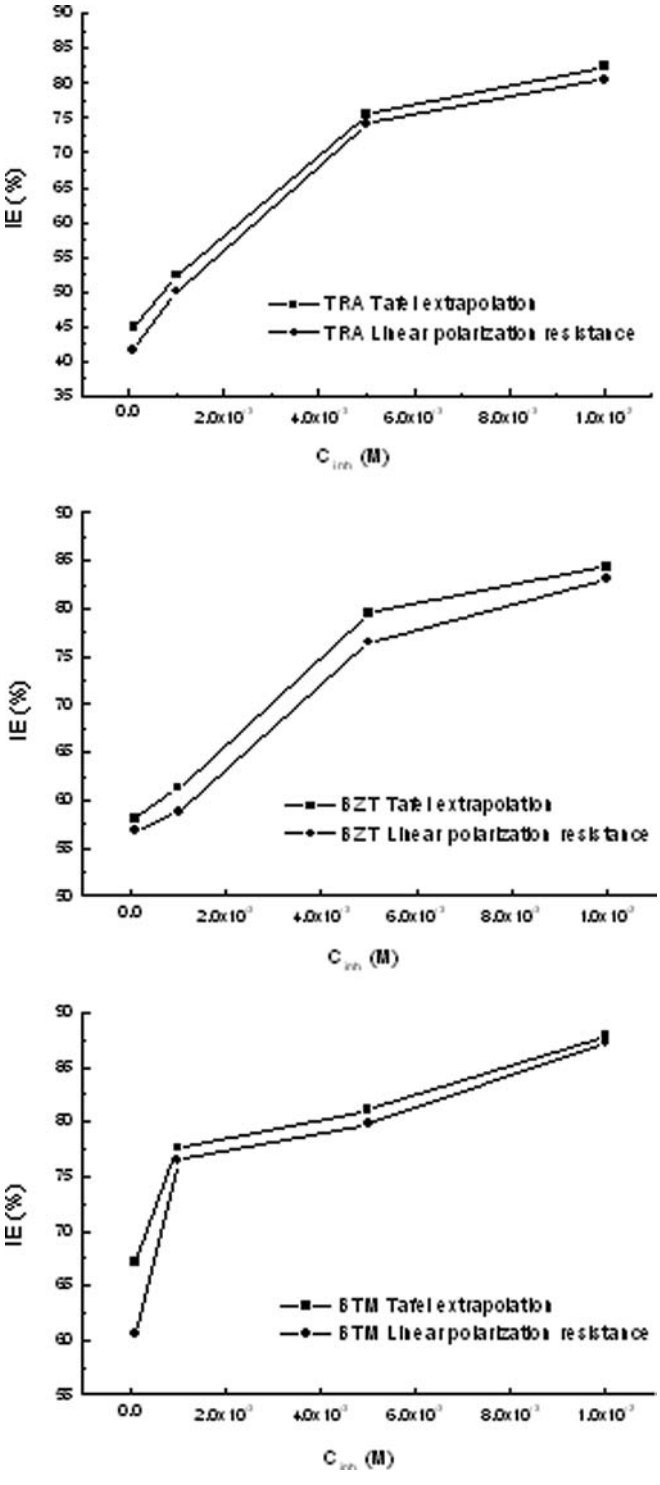

Fig. 5 DC techniques (Tafel extrapolation and linear polarization resistance) correlation graphs of inhibitor efficiency (IE%) and inhibitor concentration for TRA, BZT, and BTM in 1 mol/l HCl

and Bode-phase plots of iron corrosion in the presence of 10^{-3} mol/l and 10^{-2} mol/l BZT in 1 mol/l HCl and 1 mol/l $HClO_4$, respectively are shown in Figs. 10 and 11. The solution resistance is found from the real axis value at the high frequency intercept, near the origin of the plot. The real axis value at the low frequency intercept is the sum of the R_{ct} and R_s, equivalent to diameter of the semicircle. Figures 10b and 11b are Bode-phase plots for the same cell. The high frequency part of the impedance and phase angle describes the behavior of an inhomogeneous surface layer, while the low frequency contribution shows the kinetic response for the charge transfer reaction [24]. The phase angle does not reach 90° as it would for pure capacitive impedance [16].

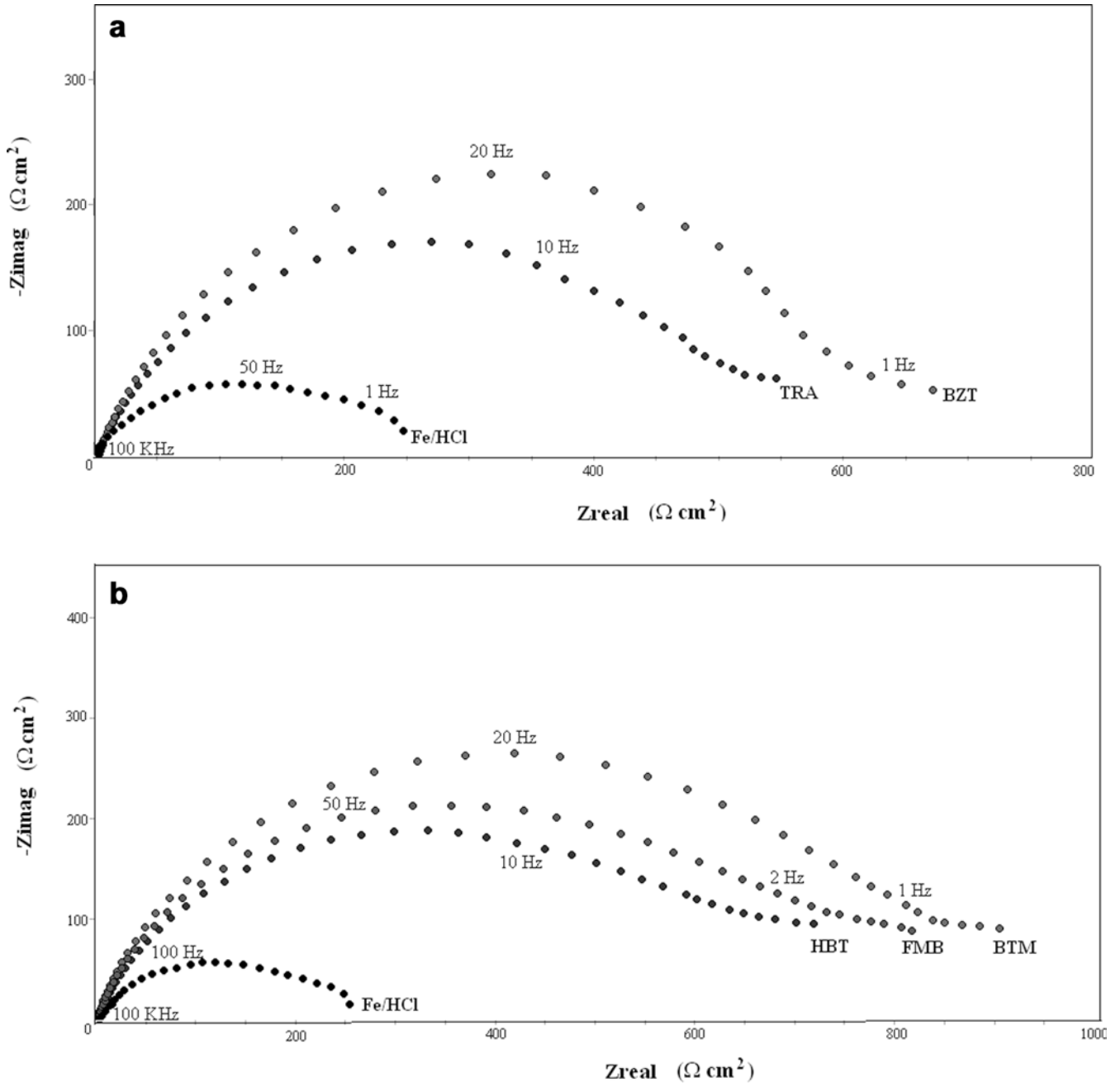

Fig. 6a,b Nyquist plots of iron in 1 mol/l HCl with: **a** 10^{-3} mol/l TRA and BZT; **b** 10^{-2} mol/l HBT, FMB, and BTM. Frequency range from 100 kHz to 0.1 Hz

Adsorption isotherm

The adsorption of the compound studied here can occur either directly through π-electrons and the *d*-orbitals of iron surface atoms or with additional interaction of the functional group. Also, there is a possibility to promote inhibition by the chloride ions already adsorbed on the surface.

By virtue of donor-acceptor interactions adsorption can occur directly through π-electrons of the triazole, benzotriazole and its derivatives and vacant *d*-orbitals of Fe atoms from the surface. Actually, triazole derivatives behave better as σ/π-donors [25]. BZT molecule is protonated in acid to form $BZTH^+$. Protonation of benzotriazole induces a decrease of its π orbital energies and the interaction between *d*- metal and its π(BZTH)-orbital decrease, leading to the lowering of the molecule resonance energy [25].

Nitrogen atoms are available for interaction sharing their electrons. Thus, each compound is chemisorbed on the iron surface through the nitrogens from the triazole ring. It is evident that the benzene ring enhances effectiveness, e.g., in 1 mol/l HCl TRA is less effective than other benzotriazoles (Table 1). The presence of oxygen-

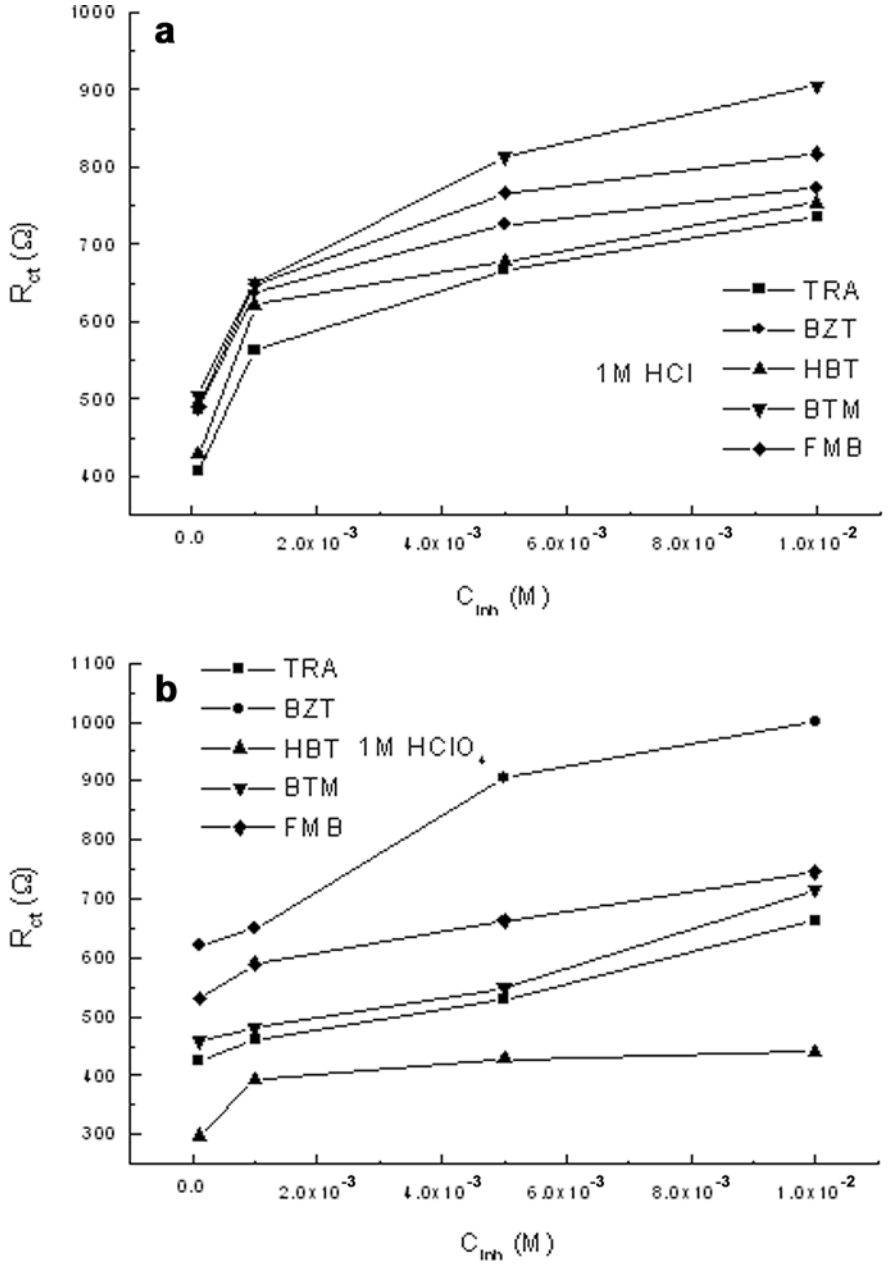

Fig. 7a,b Correlation between charge transfer resistance (R_{ct}) and inhibitor concentration in: **a** 1 mol/l HCl (Fe/1 mol/l HCl $R_{ct} = 250.5\ \Omega$); **b** 1 mol/l $HClO_4$ (Fe/1 mol/l $HClO_4$ $R_{ct} = 295.1\ \Omega$). Immersion time 900 s

containing R-groups improves inhibitor efficiency by a bit (BTM, FMB) and decrease efficiency if oxygen is directly bonded to the triazole N3-nitrogen as in HBT.

Another possibility is through electrostatic interaction between the cationic forms and a negatively charged metal surface. The effect is more pronounced if chloride anions are present [6]. With perchlorate ion a lesser interaction may lower adsorption, change molecule orientation and reduce inhibitor efficiency. Chloride ions have a stronger tendency to adsorb than do perchlorate ions. These can adsorb on the metal surface creating oriented dipoles and consequently increase adsorption of the organic cations present [26]. Also, ClO_4^- are said to have a strong effect on the molecular organization of water [27], i.e., stronger interactions with water molecules than water with itself, perhaps breaking some hydrogen bonds. Additionally, organic compounds could participate in forming of hydrogen bond network [27].

The formation of a surface 'complex film' with Fe and the triazoles is believed to provide a more compact barrier layer leading to higher inhibitor efficiency [7]. Because the derivatives of benzotriazoles are structurally different compared with basic $BZTH^+$ they probably interact more effectively on the iron surface, covering more sites and hence give better inhibition.

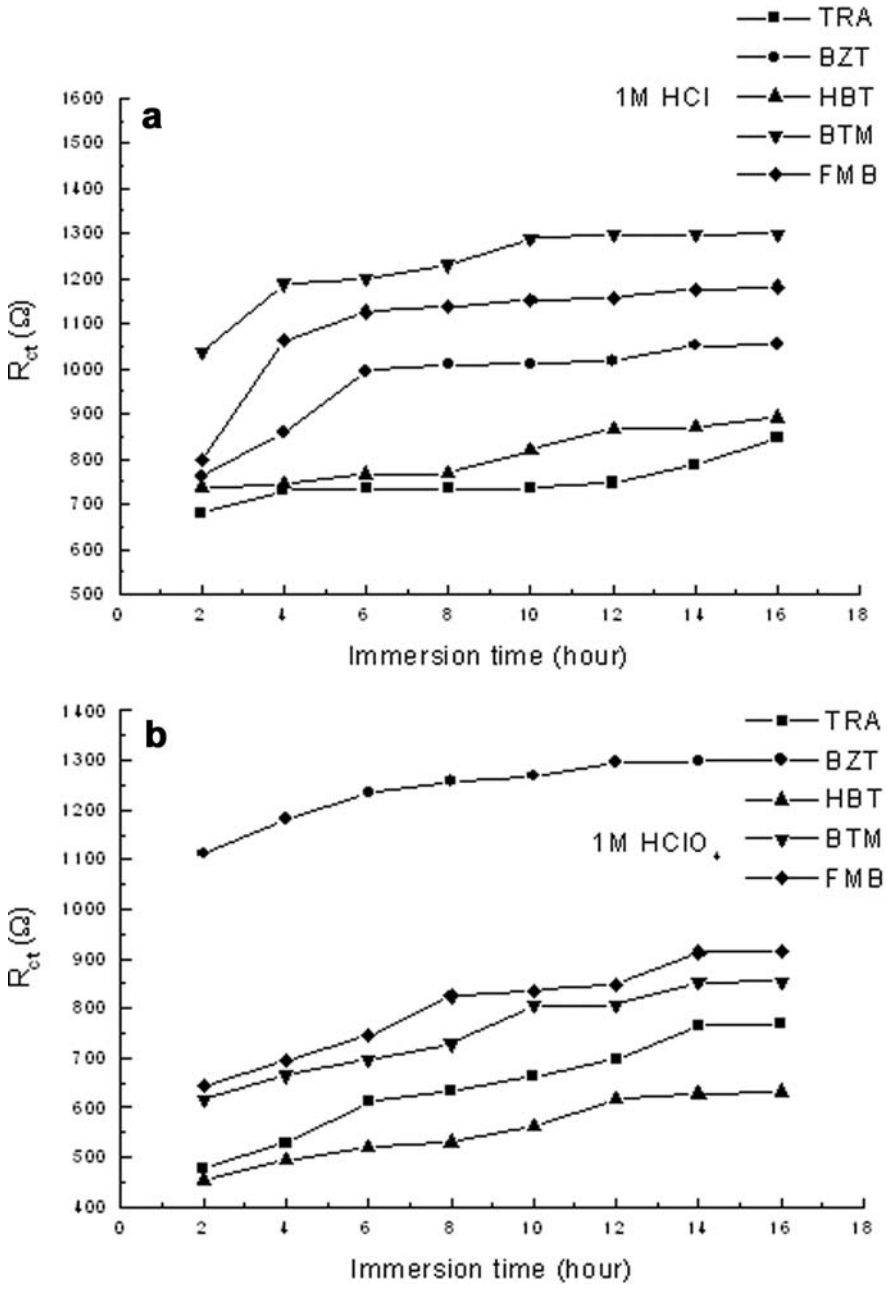

Fig. 8a,b Correlation between charge transfer resistance (R_{ct}) and immersion time (2–16 h) for Fe in: **a** 1 mol/l HCl; **b** 1 mol/l $HClO_4$ in the presence of the inhibitors studied

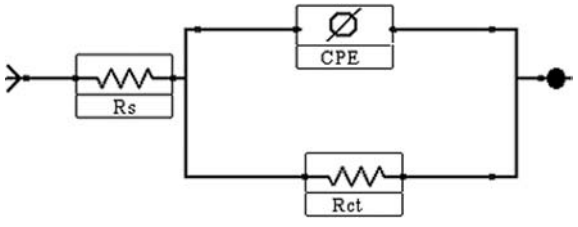

Fig. 9 Equivalent circuit model for the studied inhibitors

Assuming that the corrosion inhibition was caused by the adsorption of these molecules, the degree of surface coverage (θ) for different inhibitor concentrations was evaluated from EIS measurements using Eq. (6):

$$\theta = \left(\frac{\frac{1}{R_{ct}^{o}} - \frac{1}{R_{ct}}}{\frac{1}{R_{ct}}} \right) \quad (6)$$

Then the Langmuir adsorption isotherm was applied following Eq. (7):

$$\frac{C_{inh}}{\theta} = \frac{1}{k} + C_{inh} \quad (7)$$

where k is adsorption coefficient. The linear regression between C_{inh}/θ and C_{inh} gives data fit with high linear correlation coefficient ($R = 0.99$) (Fig. 12). The Langmuir adsorption isotherm suggests that the protonated triazole species are adsorbed in monolayers,

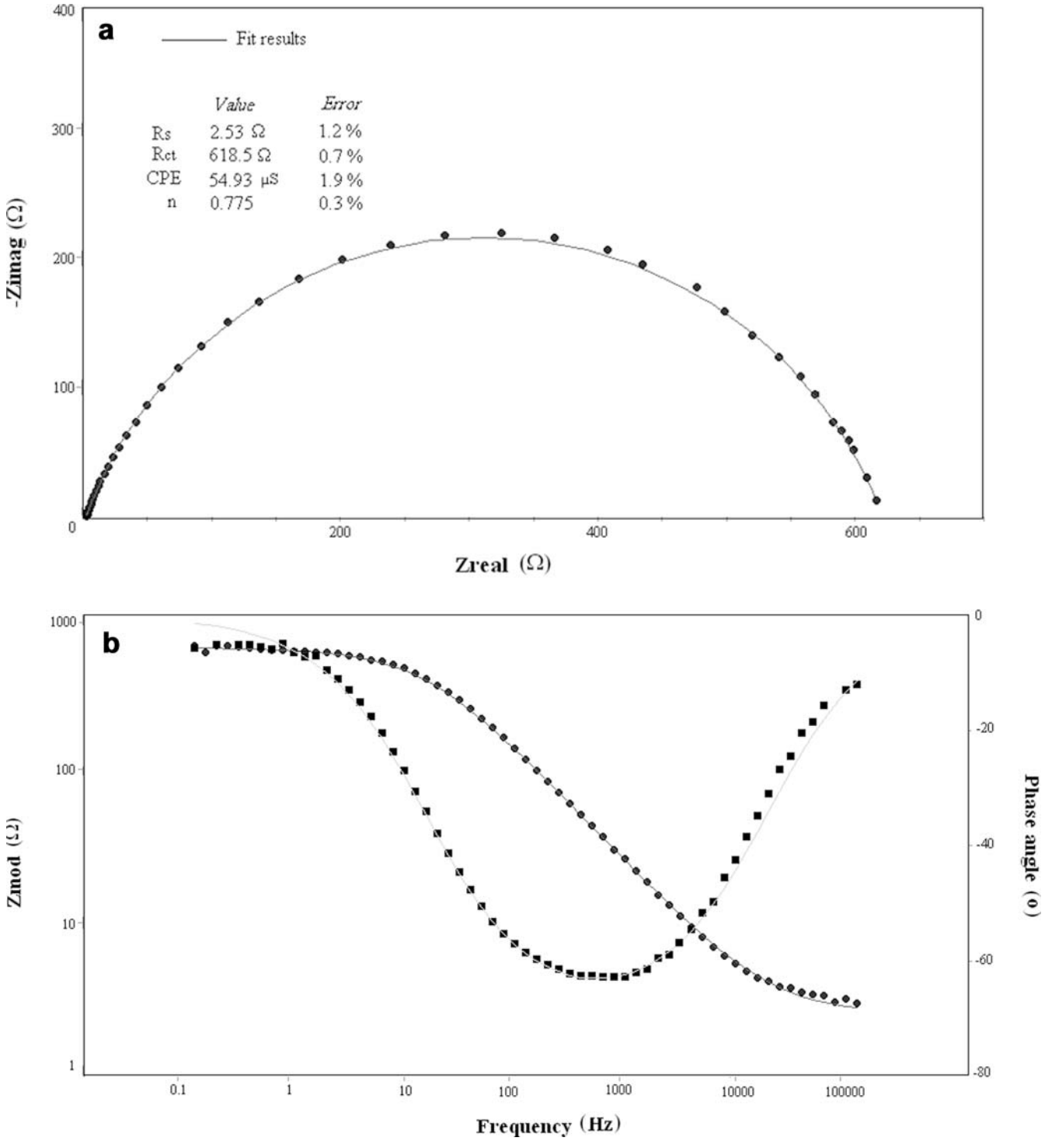

Fig. 10. **a** Nyquist plot of iron corrosion in 1 mol/l HCl in the presence of 10^{-3} mol/l BZT at E_{corr}. **b** Bode-phase plots of iron corrosion in 1 mol/l HCl in the presence of 10^{-3} mol/l BZT at E_{corr}

and the interaction with adjacent molecules is minimal [28].

The order of efficiency in benzotriazole group of compounds is different in HCl and in $HClO_4$. In 1 mol/l HCl BTM and FMB are more efficient inhibitors than BZT but in 1 mol/l $HClO_4$ the order is reversed. Probably the presence of oxygen containing fragments of benzotriazole lower the effectiveness in $HClO_4$. It is supposed to be increasing disorder of the layer(s) association close to the iron surface, which consequently leading to their decreased efficiency compared with BZT.

Some insight into their behavior is evaluated from experiments in 1 mol/l $HClO_4$ in the presence of 1 mol/l NaCl. Using the same electrochemical techniques with

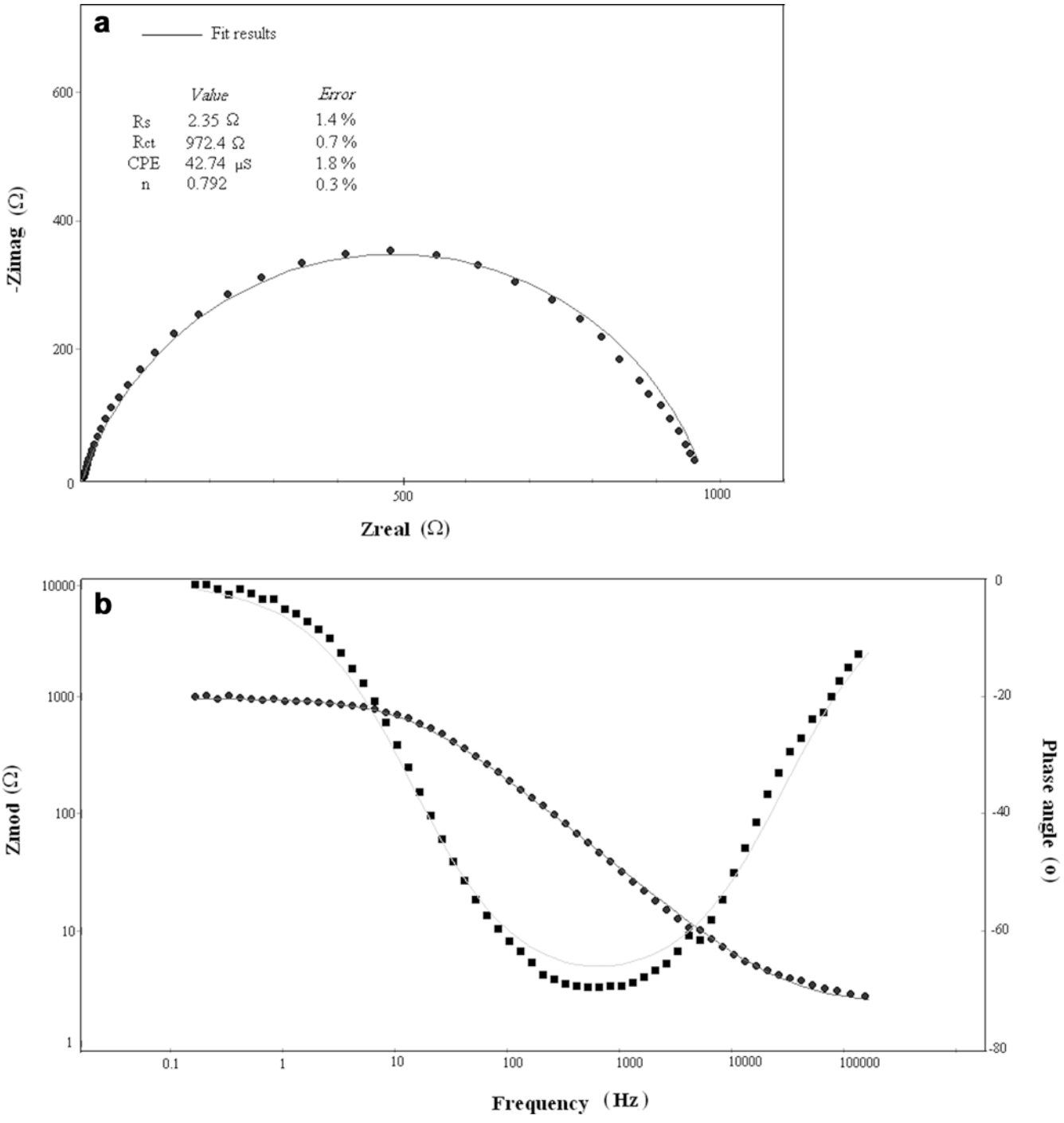

Fig. 11. **a** Nyquist plot of iron corrosion in 1 mol/l HCl in the presence of 10^{-2} mol/l BZT at E_{corr}. **b** Bode-phase plots of iron corrosion in 1 mol/l $HClO_4$ in the presence of 10^{-2} mol/l BZT at E_{corr}

this acid in presence of 10^{-2} mol/l inhibitors, the order of compound efficiency is the same as in 1 mol/l HCl. However, corrosion rates were higher than either acid alone. It is not uncommon for the presence of chlorides to enhance the effects of the inhibitor present [29]. The mechanism has been reported to be a synergistic interaction between the chloride ion and the organic molecule. In this case a positive synergistic effect arises, which is used here to explain their higher inhibitor efficiency in HCl than $HClO_4$ of same molarity.

Molecular modeling and experimental corrosion inhibition

Molecular modeling was used for better insight in the structural differences and electronic effects. Optimization of a number of parameters was performed using the PM3 SCF-MO method [17].

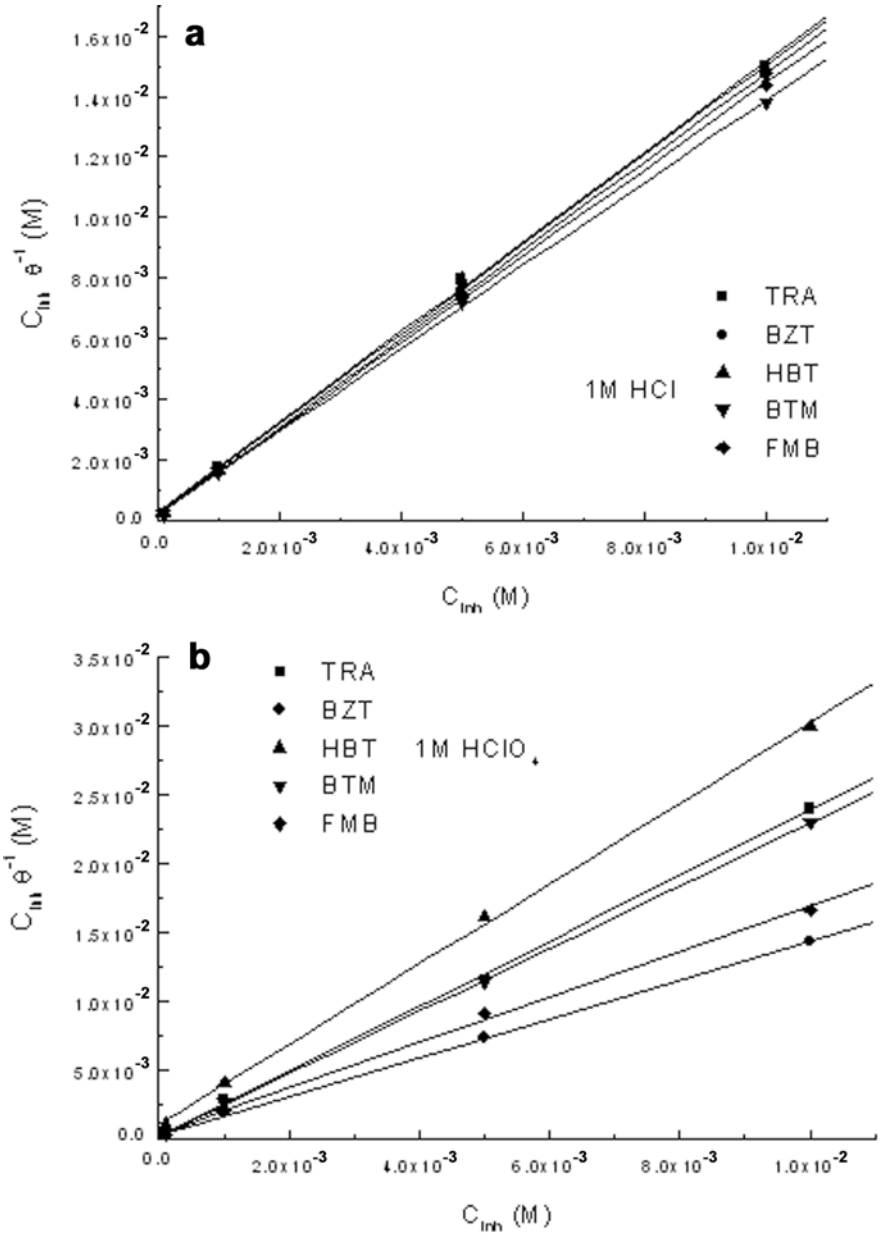

Fig. 12a,b Langmuir adsorption isotherms for compounds studied in: **a** 1 mol/l HCl; **b** 1 mol/l $HClO_4$

Generally, nitrogen atoms from the triazole ring are mainly responsible for their interaction with iron but the presence of the benzene group is not negligible. The difference between the benzotriazoles used here arises from their R-groups as well. The presence of hydroxy- (HBT), methylhydroxy- (BTM) or formamido-methylhydroxy- (FMB) groups attached to the N3-nitrogen of the aromatic triazole ring (Fig. 1) affect some structural and electronic properties of the molecule.

In the structural view it is observed that N-N bond distances inside the triazole ring are different. Electron-withdrawing hydroxy-group attached directly to N3-nitrogen in HBT increase the N2-N3 bond from the 1.372 Å as it is in BZT to 1.464 Å. There is a smaller effect in BTM and FMB (1.404 Å). The electronic effect, defined as the charge on nitrogen as well as the net charge sum of five atoms in N-cyclic ring, shows a more negative charge from BTM and FMB derivatives than BZT (Fig. 13). Also, their dipole moments (~2.5 D) are lower than all of the other three; for BZT it is 3.85 D and for TRA and HBT 4.5 D. These are directly correlated to the inhibiting behavior found in 1 mol/l HCl, i.e., in increasing order of efficiency from BTM > FMB > BZT > HBT > TRA. The resulting linear correlation between IE and charge (Fig. 13) for these compounds suggests that the electronic effect of the molecule as well as structural differences may be used to define their inhibiting performance.

Conclusions

Tafel extrapolation, linear polarization resistance and electrochemical impedance spectroscopy measurements

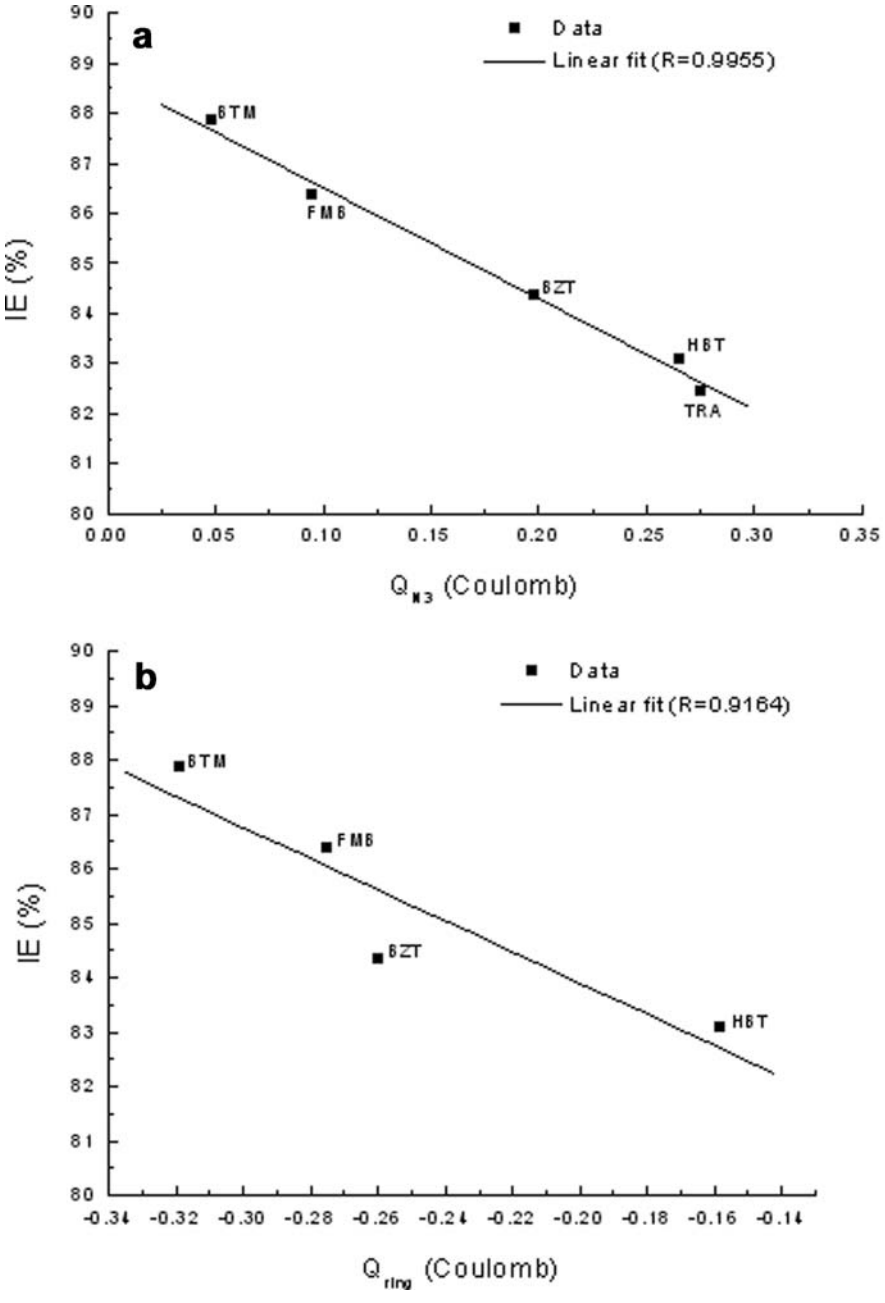

Fig. 13a,b Correlation between inhibitor efficiency vs: **a** charge of the N3-nitrogen (Q_N); **b** sum of the ring charge (Q_{ring})

were used to study iron corrosion in 1 mol/l HCl and 1 mol/l $HClO_4$ acids and the inhibiting effects of some triazole-type compounds. Analysis of the experimental data leads us to the following conclusions:

1. All investigated compounds, i.e., triazole, benzotriazole and its oxygen-containing derivatives show fair to good inhibiting properties in 1 mol/l HCl and 1 mol/l $HClO_4$.
2. Inhibiting efficiency increases with inhibitor concentration between 10^{-4} mol/l to 10^{-2} mol/l up to about 88%. Generally the inhibiting effect is higher in 1 mol/l HCl than in 1 mol/l $HClO_4$.
3. Tafel behavior indicates that the inhibitors are predominantly mixed-type.
4. The inhibiting efficiency increases with increasing of immersion time up to 16 h.
5. The inhibiting effect is more pronounced in 1 mol/l HCl, and the inhibitor efficiency increases according to order, BTM > FMB > BZT > HBT > TRA.
6. In 1 mol/l $HClO_4$, inhibiting effect of benzotriazole is better than its derivatives, BZT > FMB > BTM > HBT.
7. The Langmuir adsorption isotherm appears to describe their adsorption behavior in both acids.
8. The results are discussed in terms of structural and electronic parameters obtained via molecular modeling.

Supplementary material is available upon request from the corresponding author for all experimental details, which are not tabulated and presented in this paper.

Acknowledgement The authors are pleased to acknowledge the financial support provided by the Robert A. Welch Foundation of Houston, Texas, USA.

References

1. Roberge PR (1999) Handbook of corrosion engineering. McGraw-Hill
2. Ramesh S, Rajeswari S (2004) Electrochim Acta 49:811
3. Al-Mayouf AM, Al-Ameery AK, Al-Suhybani AA (2001) Corrosion 57:614
4. Tamil Selvi S, Raman V, Rajendran N (2003) J Appl Electrochem 33:1175
5. Chebabe D, Ait Chikh Z, Hajjaji N, Srhiri A, Zucchi F (2003) Corros Sci 45:309
6. Lagrenee M, Mernari B, Bouanis M, Traisnel M, Bentiss F (2002) Corros Sci 44:573
7. Bentiss F, Lagrenee M, Traisnel M, Hornez JC (1999) Corros Sci 41:789
8. Aksut AA, Onal AN (1997) Corros Sci 39:761
9. Bartley J, Huynh N, Bottle SE, Flitt H, Notoya T, Schweinsberg DP (2003) Corros Sci 45:81
10. Trasatti S (1992) Electrochim Acta 37:2137
11. Matos JB, D'Elia E, Barcia OE, Mattos OR, Pebere N, Tribollet B (2001) Electrochim Acta 46:1377
12. Gomma GK (1998) Mater Chem Phys 56:27
13. Lim MS, Perry SS, Galloway HC, Koeck DC (2003) Tribology Lett 14:261
14. Da Costa SLFA, Rubim A, Agostinho SML (1987) J Electroanal Chem 220:257
15. Yao JL, Ren B, Huang ZF, Cao PG, Gu RA, Zhong-Qun T (2003) Electrochim Acta 48:1263
16. Macdonald DD, McKubre MCH (1996) Electrochemical impedance techniques in corrosion science, electrochemical corrosion testing. Mansfield F, Bertoci U (eds). STP 727, ASTM, Philadelphia
17. Stewart JJP (1989) J Comput Chem 10:209
18. Roothaan CCJ (1951) Rev Mod Phys 23:69
19. Thiel W (2000) Modern methods and algorithms of quantum chemistry. NIC Series 3:261
20. Wolinski K, Hinton JF, Pulay P (1990) J Am Chem Soc 112:8251
21. Dewar MJS, Liotard DA (1990) J Mol Struct (Theochem) 206:123
22. Huynh N, Bottle SE, Notoya T, Trueman A, Hinton B, Schweinsberg DP (2002) Corros Sci 44:1257
23. Stern M, Geary AL (1957) J Electrochem Soc 104:56
24. Khaled KF, Hackerman N (2003) Mater Chem Phys 82:949
25. Rocha RC, Toma HE (2001) Inorg Chem Commun 4:230
26. Lorenz WJ (1970) Z Phys Chem 65:244
27. Koga Y, Westh P, Nishikawa K (2004) J Phys Chem A 108:1635
28. Tang L, Mu G, Liu G (2003) Corros Sci 45:2251
29. Li P, Lin JY, Tan L (1997) Electrochim Acta 42:605